Morphologies of Polyisoprene Grafted Silica Nanoparticles in Model Elastomers

Marine Bonnevide, a,b,c Andrew M. Jimenez, Deboleena Dhara, Trang N.T. Phan, Nicolas Malicki, Zaid M Abbas, Frian Benicewicz, Sanat K. Kumar, Marc Couty, Didier Gigmes, and Jacques Jestin a,*

^a Laboratoire Léon Brillouin, UMR 12, Université Paris-Saclay, IRAMIS/CEA Saclay 91191 Gif-sur-Yvette Cedex France

^b Aix Marseille Univ, CNRS, Institut de Chimie Radicalaire, UMR 7273-Campus Scientifique St Jérôme, Service 542 13397 Marseille Cedex 20, France Marseille, France

^c Manufacture Française des Pneumatiques MICHELIN, Site de Ladoux, 23 place des Carmes Déchaux, F-63 040 Clermont-Ferrand, Cedex 9, France

^d Department of Chemical Engineering, Columbia University, New York, New York 10027, United States

^e Department of Chemistry and Biochemistry, University of South Carolina, Columbia, South Carolina 29208, United States

^f Department of Chemistry, Wasit University, Hay Al-Rabea, Kut, Wasit, 52001, Iraq

ABSTRACT

We control nanoparticle dispersion by leveraging the entropic and enthalpic effects associated with mixing silica nanoparticles (NPs) grafted with polyisoprene (PI) chains into matrices of varying degrees of chemical dissimilarity. Previous work in this area has primarily focused on entropic factors alone, and hence this work represents a significant advance over the current state-of-theart. We show using a combination of transmission electron microscopy (TEM)/small angle x-ray scattering (SAXS) that mixing grafted particles with polyisoprene matrices of identical microstructure yields dispersion states as found in the literature for such entropic systems. However, replacing the PI matrix chains with dissimilar matrices leads to an introduction of enthalpic interactions that, in some cases, can drastically change the resulting morphology. In particular, while slightly different PI microstructures for the grafted and free chains only yield quantitative differences, using styrene-butadiene copolymers as a matrix leads to completely different behavior. In the last case, phase separation becomes more likely with increasing graft length, while the PI system (whose behavior is dominated by entropic factors) shows the opposite behavior. Tuning the relative importance of enthalpic vs. entropic factors is thus another tool in controlling the self-assembled structure of NPs, which give rise to enhanced macroscopic properties in the composite.

I Introduction and Background

The addition of inorganic nanoparticles (NPs) to polymer matrices is a widely-used strategy to improve the electrical¹, optical², mechanical³, flame retardancy⁴ or gas barrier⁵ properties. This improvement of properties is related to the specific contact area between fillers and matrix which increases as the particles size decreases (at fixed loading), so long as the particles maintain the same state of dispersion⁶⁻⁹. Generally, adding ~5%wt. of 10 nm filler allows one to obtain the same mechanical property enhancement as with 30%wt. of micron-sized particles 10. However, NPs tend to aggregate, i.e., the dispersion gets progressively worse with decreasing NP size, resulting in a reduction of the specific contact area with the matrix¹¹ with deleterious effects on final properties¹². Over the last few years, significant efforts have been made to develop new strategies for controlling the NP dispersion, in particular by grafting the NP with polymer chains with the same chemistry as the matrix; variations of the grafting densities and the ratio of the lengths of the grafted (N) and free (P) chains allows one to access a range of NP dispersion states 13, 14. Kumar et al. used a compilation of experiments and numerical simulations on conventional polymers (PS, PMMA, where the grafts continue to have the chemical structure as the matrix), to delineate regions in parameter space where individual NP dispersion, phase separation, small clusters and connected sheets form¹⁵. While these results are interesting, it is critical to examine if these findings have relevance to commercially relevant elastomeric systems, where the grafts and matrices may not always have the same chemical (micro) structure 16, 17. Among the various elastomers, polyisoprene (PI) and its copolymers are of great interest and are used for medical applications^{18, 19}, sporting goods²⁰ and in the automotive industry²¹⁻²³ due to their excellent break, wear and tear strengths.

It is important to stress that NP agglomeration can be even more important in these practically important situations because of the very poor energetic interactions between typical NPs and elastomers²⁴. Previously, several solutions have been proposed to improve the dispersion of NPs in elastomers. Bouty et al.^{25, 26} studied the dispersion of silica NPs with an average radius of 8 nm in SBR (styrene-butadiene rubber) by modifying the surface with (i) a coupling agent (bis(triethoxysilyl)propyl tetrasulfide) which can covalently bond with the matrix chains via the sulfur bond, or (ii) a coating agent (octyltriethoxysilane) which is known to improve the enthalpic compatibility with the polymer. They demonstrated that the coupling agent leads to smaller aggregates as compared to the coating agent which yields larger and ramified objects, though neither approach allowed them to obtain individual NP dispersion. A similar approach was also investigated by Baeza et al.²⁷ using functionalized SBR chains, and *in situ* grafting the SBR chains to the NPs. Such approaches are strongly limited by the reaction of the chains to the NP surfaces. To circumvent this limitation, one can use controlled polymer grafting of the particle (as previously described for conventional polymers) before the NPs are dispersed in the matrix. Hosseini et al.²⁸ compared the effects of modifying precipitated amorphous silica (specific surface area of 180 m²/g) with a coupling agent or with hydroxyl-terminated polybutadiene (HTPB) of 2800 g.mol⁻¹. They showed that the dispersion of silica in a SBR matrix was more uniform and homogeneous when it was modified with HTPB but this grafting also led to a worsening of mechanical properties, presumably due to a disruption of the filler network and the lack of strong filler polymer bonding. These results however assert that it is necessary to optimize and control grafting parameters such as grafting density and chain length to obtain the optimal dispersion state for improved mechanical properties. To our knowledge, the only example of surface polymerization of isoprene on to silica NPs using a reversible-deactivation radical polymerization (RDRP) technique was recently

reported by Khani et al.²⁹. They first synthesized chain-transfer agent functionalized silica NPs and then polymerized isoprene onto the surfaces using reversible addition fragmentation chain transfer (RAFT). They also studied the dispersion of PI-grafted SiO₂ NPs in a PI matrix using TEM and showed compatibility between the grafted NPs and the matrix. In the current work we present the compatibility of PI-grafted SiO₂ synthesized from both Surface Initiated (SI)-RAFT as well as nitroxide mediated polymerization (NMP) in "grafting from" polymerizations of isoprene from silica NPs. The combination of different techniques such as thermogravimetric analysis (TGA), Small Angle Neutron Scattering (SANS) and Size Exclusion Chromatography (SEC) allows for a detailed characterization of these polymer-grafted NPs, namely the resulting grafting density and chain length³⁰. Subsequently, we studied their dispersion in elastomeric matrices of different microstructures using SAXS and TEM showing an evolution of dispersion depending on the grafting density and the ratio of the matrix chain length and the grafted chain length.

II Material and methods

1 Materials

Spherical SiO₂ nanoparticles (TOL-ST and MEK-ST), with a nominal diameter of 10-15 nm, were provided by Nissan Chemical Company. Ultracel® membranes (30kDa, 100kDa, Merck Millipore), 2-(((dodecylthio)carbonothioyl)thio)propanoic acid (DoPAT) (Strem Chemicals, 97%), Tetrahydrofuran (THF) (Carlo Erba Reagents, 99.9%; Fisher, HPLC), pentane (VWR, 95%), N_iN_i -dimethylacetamide (Aldrich, 99.9%), Dicumyl peroxide (Aldrich, 99%), Dimethylmethoxy-n-octylsilane (Gelest, 95%), 3-aminopropyldimethylethoxysilane (Gelest, 95%), anhydrous methanol (Aldrich, 99.8%), isoprene (Aldrich, 99%) and polyisoprene, cis (Aldrich, M_w =35000g/mol) were used as received.

2 Sample preparation

The grafted nanoparticles were synthesized using two techniques to produce PI grafted silica NPs: SI-RAFT²⁹ and NMP³⁰, designated PI-RAFT-SiO2 and PI-NMP-SiO2, respectively. RAFT synthesis was also used to provide free PI chains of the same microstructure as the NP grafted chains, designated PI-RAFT (further details on synthesis are included in the Supporting Information). Additional free polymer chains purchased from Sigma were used as a matrix of dissimilar microstructure, designated PI-Sigma and Styrene-Butadiene-Rubber SBR (*Mw*=54kDa, 26% styrene; 31% PB 1,2; 23% PB-1,4 trans; 20% PB 1,4 cis, dispersity=1.1) provide by Michelin. The microstructures of each can be found in Table 1. The effects from mixing the various microstructures are described in the subsequent results.

 Table 1: Polyisoprene Microstructure

	Mw	Đ	% 1,4 trans	% 1,4 cis	% 1,2	% 3,4
	(kDa)	(Dispersity				
		index)				
PI-RAFT-SiO2	28-120	1.4-2.1	75	20	1.3	3.7
PI-NMP-SiO2	20-45		43.7	24.6	13.2	18.6
PI-RAFT	52	1.8	75	20	1.3	3.7
PI-Sigma	35	3.5-4	24.8	75.2	-	-

Composite samples were solution cast by dissolving free matrix chains at 5 wt% in THF before adding PI grafted NPs at ~5 wt% NP core (SiO₂) to the total mass. The resulting mixture was vigorously stirred/vortexed for 2-4 hours at room temperature, and then probe sonicated before

allowing the THF to slowly steadily evaporate off (without boiling), under vacuum, again at room temperature.

Our previous work³¹ has shown that the NP structures that form, especially in the case of large graft densities, are independent of the particular solvent employed as long as it is favorable to the graft chains. This is likely because the grafts shield the NP core and thus ensure good dispersion in the initial state obtained after solvent casting. In agreement with these notions we find similar NP structures when toluene or THF are used in sample preparation; on the other hand, xylene (a poor solvent for the grafts) yields agglomerated NPs.

3 Scattering and microscopy characterization

3.1 Small Angle X-Ray Scattering (SAXS) and USAXS

SAXS experiments were carried out on a Xeuss 2.0 apparatus (Xenocs, France) at the Laboratory Léon Brillouin (LLB NIMBE CEA Saclay). The instrument uses a microfocused Cu K_{α} source with a wavelength of 1.54 Å and a Pilatus3 detector (Dectris, Switzerland). The experiments were performed with a collimated beam size of 0.3 x 0.25 mm. The sample-to-detector distance was chosen to be 2540 mm to achieve a Q range of 0.004 to 0.2 Å-1. Additional SAXS was performed on a Saxslab Ganesha instrument (Xenocs, France) at the Columbia Soft Matter Laboratory, with the same Cu K_{α} source and effective Q range. The elastomer films were molded into an aluminum ring and sealed between two Kapton sheets. Scattering from empty beam, Kapton sheets and dark field were measured independently and subtracted using standard protocols. The data were normalized to absolute units. Modelling and fitting were performed with the SASFIT software. USAXS experiments were carried out on the beamline ID02 at ESRF (Grenoble), with a

wavelength of 1 Å (E = 12.4 keV) and two sample-to-detector distances of 1 and 30 m, yielding a total Q range from 2×10^{-4} to 5×10^{-1} Å⁻¹.

3.2 Transmission Electronic Microscopy (TEM)

Samples were cut from the un-crosslinked melt using cryo-ultramicrotomy and imaged using cryo and room temperature TEM. Cryo-ultramicrotomy was performed on a Leica EM FCS microtome at -90 °C with cut speeds varying between 2-10 mm/s to obtain sections of thickness ~100 nm. The sections were collected on a Formvar coated copper grid and stored in liquid nitrogen prior to imaging on an FEI Talos 120C TEM at 120kV, equipped with a Gatan OneView camera.

3.3 Differential Scanning Calorimetry (DSC)

DSC analyses were performed on a TA Instruments (DSC Q20) with the following program (heat-cool-heat cycle): heat from 25°C to 50°C at 10°C/min, cool to -80°C at 10°C/min and heat to 50°C at 10°C/min. Heat curves from the second heating are used here.

III Results and discussion

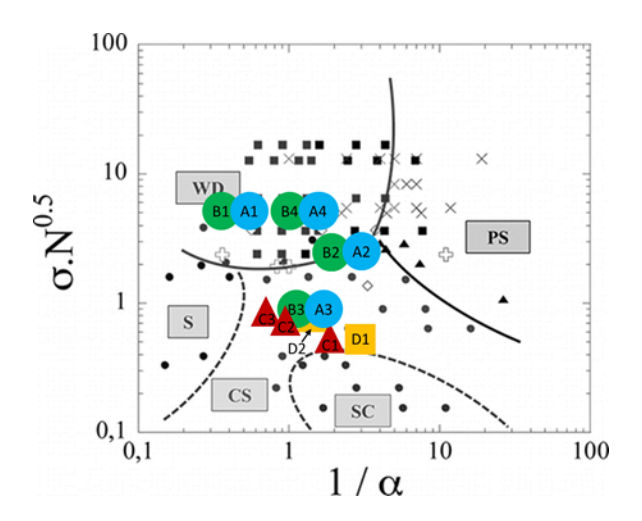


Figure 1: Morphology diagram of polymer grafted nanoparticles in a polymer matrix, borrowed from Kumar et al.¹⁵. Samples in color represent the various systems studied in this work: (blue circle) PI-RAFT-SiO₂ in PI-RAFT matrix, (green circle) PI-RAFT-SiO₂ in PI-Sigma matrix, (red triangle) PI-NMP-SiO₂ in PI-Sigma matrix, and (yellow square) PI-NMP-SiO₂ in SBR matrix. Data on smaller green circles can be found in the SI. (WD = well dispersed, PS = phase separated, CS = [Connected] Sheets, SC = Small Clusters, S = Strings. Note: $\alpha = N/P$).

The morphology diagram shown in Figure 1 is a common reference point for helping to determine a priori what kind of NP dispersion one can expect for polymer grafted NPs in a polymer matrix $(\sigma = \text{graft density}, \alpha = N/P, \text{ where } N = \text{degree of polymerization of the grafted chain and } P =$ degree of polymerization of the matrix, see Table 2). This empirical plot is the compilation of data from a variety of polymeric systems, but is largely dominated by the athermal system of PS-gsilica in PS matrix, guided by the theoretical principles from Akcora et al.³¹. The N and P values used here are based on the recorded weight average molecular weights, M_w , of the polymers. For highly uniform polymers (low dispersity, D), the application of this morphology diagram is largely unaffected by the choice of reported molecular weights. However, industrially purchased polymers often report D values in the range of 2-4, which could significantly change the expected morphology. For completeness, we include the same plot in the Supporting Information using instead the number average molecular weight, M_n . While some papers suggest the use of M_n to more accurately represent the system, we chose to focus here on M_w to capture the influence of the addition of long chains in highly disperse systems. Regardless of molecular weight definition, these systems can experience a transition from dispersed to agglomerated through either decreased wetting of a dense graft with increasing matrix chain lengths (well dispersed – phase separated), or decreasing graft density which exposes the NP core and allows for clustering due to core-core attractions (well dispersed - strings/sheets/small clusters). The latter of course depends on the core-matrix interaction, where a favorably interacting core-matrix system, with smaller van der Waals attractions, can promote good NP dispersion regardless of NP grafting. The system studied

here focuses on silica nanoparticles (hydrophilic cores with relatively low van der Waals attractions, compared to other commonly used NPs) in hydrophobic polymer matrices. While the morphology diagram appears to encompass these phenomena seamlessly, the root cause for agglomeration is necessary to distinguish, especially when looking at systems with non-zero interaction parameters (χ) between the graft and matrix. Martin et al.³² show with simulations and experiments that the wetting/dewetting process occurs gradually with changes in χ, whereas agglomeration is a sharper first order process which occurs with increases in χ. In highly unfavorable mixtures the grafted NPs can fully phase separate, despite dense polymer grafting, as one would expect to see in immiscible polymer blends like polystyrene and poly(methyl methacrylate). The present work attempts to further test the validity of this model morphology diagram when enthalpic effects due to mismatched grafted and matrix polymers being used are introduced. Through the use of two separate grafted NPs and three polymer matrices, we produce four unique systems to study: (Case A) PI-RAFT-SiO2 in PI-RAFT – the only system in which the grafted PI is identical in microstructure to that of the matrix and is therefore our athermal starting point, (Case B) PI-RAFT-SiO2 in PI-Sigma – here the microstructure of the matrix is effectively flipped in the relative ratio of 1,4 cis and trans, (Case C) PI-NMP-SiO2 in PI-Sigma – again the commercial cis PI is used as the matrix but now the grafted chain has a more diverse microstructure, and finally (Case D) PI-NMP-SiO2 in SBR – this system further probes the enthalpic effect by mixing the grafted NPs with a drastically different chemically structured polymer matrix. As is done with many other systems, these are all plotted on the polymer nanocomposite morphology diagram, which uses only the entropic parameters of graft density of chains on the NP surface and the ratio of the degree of polymerization of the grafted and free chains. Figure 1 demonstrates that with all of these systems we can cover a wide range of the

morphology diagram, stretching across more than an order of magnitude on each axis. From this, we could naively expect to find generally well-dispersed and connected sheet morphologies throughout the samples.

Table 2: Polyisoprene Grafting Parameters

	N	σ	P/N
	(kDa)	(chains/nm ²)	$(1/\alpha)$
A1, B1	104	0.15	0.50, 0.34
A2, B2	20	0.15	2.6 , 1.8
A3, B3	32	0.035	1.5 , 1.1
A4, B4	38	0.25	1.4, 0.90
C1, D1	20	0.03	1.75 , 2.88
C2, D2	38	0.03	0.92, 1.49
C3	45	0.03	0.78

1. Moving From Athermal to Mismatched Graft/Matrix Microstructures

As a control case, the PI-RAFT-SiO2 NPs were first mixed with PI-RAFT free polymers of the same microstructure (75% 1,4 trans, samples A1-A4 in Table 2). We focus first on four "A" samples (Table 2), taking us from deep within the well dispersed region (moderately high graft density, long grafted chains, A1), out to the edge of the phase separated transition (high graft

density, short grafted chains, A4), down slightly toward sheets (moderate graft density, short grafted chains, A2), and finally deep into the sheet forming region (low graft density, short grafted chains, A3). (Long and short chains are relative to the matrix molecular weights seen in Table 1). Upon TEM analysis, the NP structures appear to correspond very well with what the phase diagram predicts. The two systems sufficiently within the well-dispersed region appear as such (Figure 2 A1, A4), while the sample down in the sheet region shows high levels of agglomeration (Figure 2 A3). The sample on the edge of the boundary, though certainly agglomerating, appears to be somewhere in-between (Figure 2 A2). SAXS provides further support for these structural assignments. The well-dispersed systems exhibit structure peaks that can be fit with a Percus-Yevick structure factor. The q* dependence of the peak on NP loading supports that this change in interparticle spacing is due to NPs that are largely individually dispersed throughout the matrix (Figure 3C). Following the qualitative trends from TEM, the SAXS also shows a relative level of agglomeration between the sheet forming samples. Deep in the sheet region, the SAXS for A3 shows a low q scattering dependence of $I \sim q^{-2}$, whereas the sample near the phase transition, A2, shows scattering with a scaling exponent of ~1.5 (Figure 3A). This aligns well with the apparent difference in cluster density seen in TEM (Figure 2).

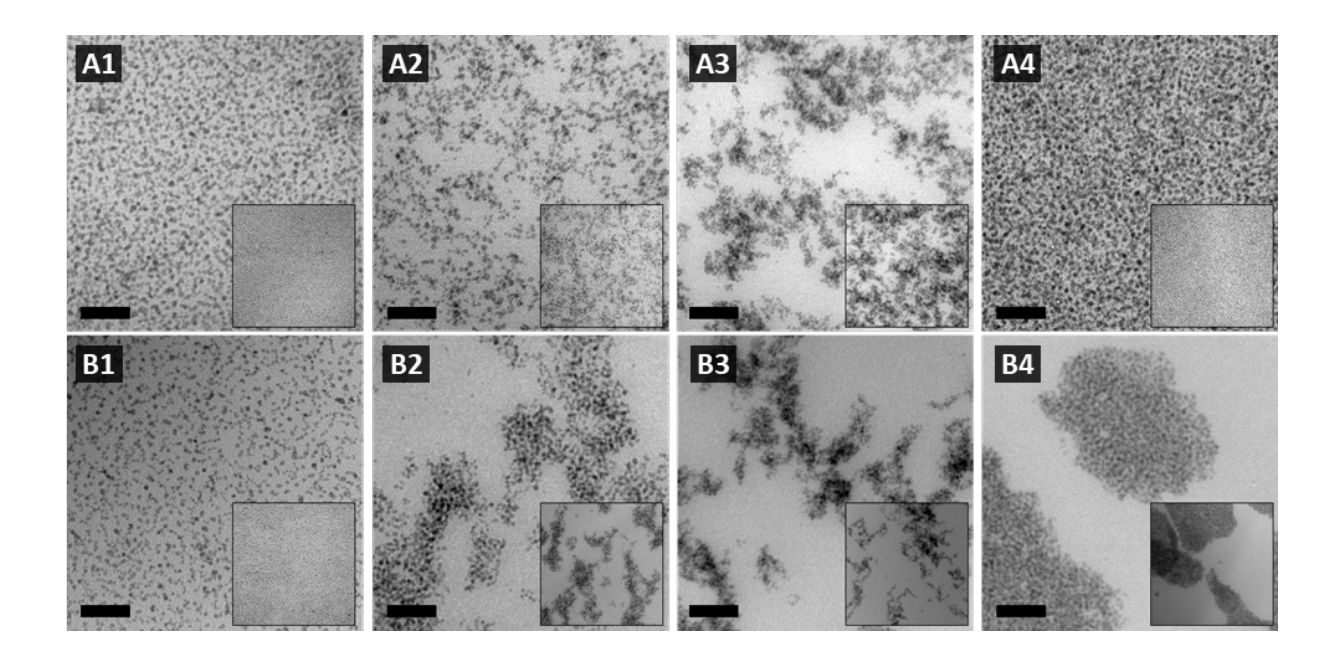


Figure 2: TEM images of PI-RAFT-SiO2 in (A#) PI-RAFT [matched] matrix and in (B#) PI-Sigma [mismatched] matrix. Samples include (X1) 104kDa at 0.15 ch/nm², (X2) 20kDa at 0.15 ch/nm², (X3) 35kDa at 0.035 ch/nm², and (X4) 38kDa at 0.25 ch/nm². Scale bar is 200 nm for the large images and 1 μm for the insets.

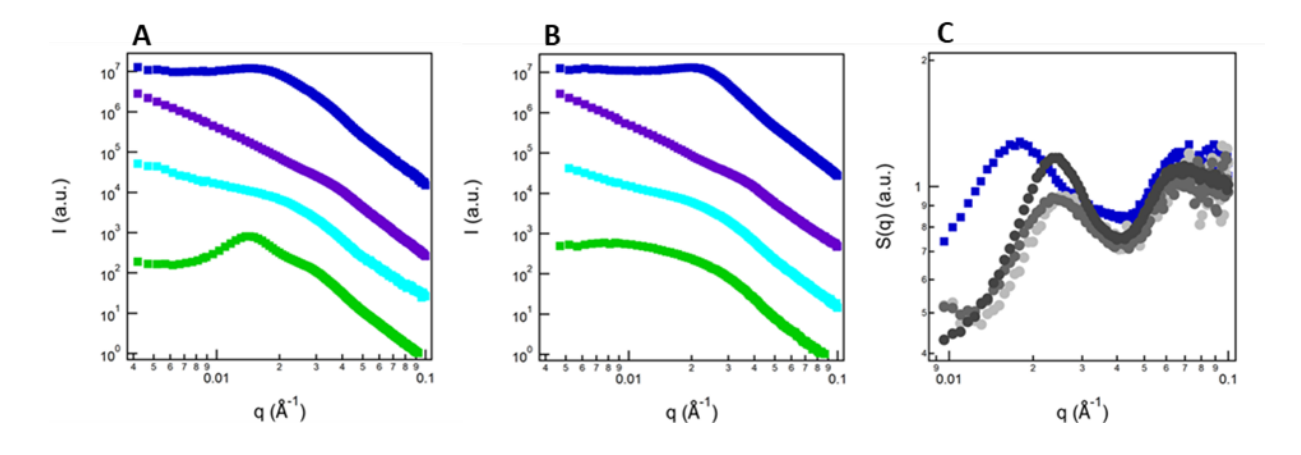


Figure 3: SAXS of PI-RAFT-SiO2 in (A) PI-RAFT [matched] matrix and in (B) PI-Sigma [mismatched] matrix. Samples include (green) A1/B1, (cyan) A2/B2, (purple) A3/B3, and (blue) A4/B4 with properties noted in Table 2. (C) SAXS structure factors corresponding to the scattering for sample (blue squares) A4 and sample (grey) B4, with increasing NP loadings for darker grey shadings (1, 5, 15 wt%).

Building from the structural assignments of the athermal system, the same NPs were then mixed into an industrial PI matrix (75% 1,4 cis) purchased through Sigma, with a notably higher polydispersity index. Upon doing so there are immediately obvious changes in only one sample – B4, the one nearest the phase separated region. Unlike the well-dispersed NPs seen throughout the

TEM section of the matched matrix sample, the PI-Sigma composite shows large, phase separated regions of NPs spanning 10s of micron (Figure B4). Changes in NP structure for the other composites is less obvious. Moving back to the left on the phase diagram, the NPs with long chains and high graft density still appear to be well dispersed (B1), though a small degree of NP stringing can be seen. As for the sheets, the relative density of agglomerates appears relatively similar for B3, but B2 may have slightly denser NP clusters than its A2 counterpart. Again, SAXS is used to further support these trends. Dividing the scattering intensity by the form factor of the NPs (measured in dilute solution) provides the structure factor, S(q) = I(q)/P(q) (Figure 3C). The composites with sheet-like aggregates (A2/B2 and A3/B3) show strong self-similarity in the NP structure formation, regardless of matrix (see Supplementary Supporting Information). This may be due to changes in the scattering only appearing at q values below the studied range for this system. Both well-dispersed samples appear to have lost some level of their dispersion, but to drastically different degrees. The "B" sample nearest the phase separated boundary, B4, displays a strong scattering peak around 0.023 Å⁻¹. Using $q = 2\pi/d$, this corresponds to a center-to-center NP spacing of 27 nm, roughly the size of the NP plus grafted shell. This spacing does not change with NP loading, suggesting phase separation (Figure 3C). The sample further from the phase separated boundary (B1) loses the strong structure peak at the expected well-dispersed NP spacing, seen in the A1 counterpart, but maintains a well dispersed NP form factor. This suggests that the NPs are still largely dispersed, though to a less uniform degree, i.e. the distribution in interparticle spacing has increased (compare Figures 3A and 3B). The change in dispersion of both initially well-dispersed samples suggests a shrinking of the well-dispersed region for this system. The slight change in interaction of the dissimilar graft-matrix polymers pushed the B4 system toward phase separation through the enthalpically driven dewetting of the grafted brush. This dewetting is likely further assisted by the increase in dispersity of the Sigma matrix, such that the increase in the number of longer chains will promote phase separation. Equally interesting is the more subtle shift in dispersion of A1 to B1. Rather than a sudden phase separation of NPs in this new matrix, we see something more similar to the string morphology, meaning we have managed to shift to different morphologies without changing N nor σ . This minor shift in morphology could suggest the ability to control the sharpness of the dispersion-agglomeration transition by varying the grafted chains, despite having similarly unfavorable interactions with the matrix.

2. Moderately Mismatched Microstructure (with NMP Synthesis), Focusing on NP Structures in the Sheet Forming Regions

To further study the effect of mismatched microstructure on dispersion, samples synthesized with a different grafting chemistry were mixed again in the industrial PI matrix and studied by SAXS, specifically focusing on the lower region of the phase diagram. The PI polymerized by NMP has a different microstructure than of both the RAFT and the Sigma PI, as determined by ¹³C NMR (Table 1). These samples have a relatively constant graft density of 0.03 chains/nm² but with grafted chain with slightly different molecular weight (and polydispersity, Table 2). In Figure 4 we show the variation in scattering intensity of the nanocomposites (the form factor of a primary particle are shown for comparison) when increasing the molecular weight of the grafted chain, keeping all other variables constant. In the high q region, all the curves more or less superimpose, implying that we are sensitive to the primary particle scattering in this q range. The behavior begins to diverge at low q, where intensity level reflects the formation of clusters comprised of primary particles. The morphology of such cluster depends directly on the number of primary particles, namely the apparent aggregation number (N_{agg}) taken from the extrapolation of the scattered

intensity plateau when q tends to zero, as well as the compactness of the clusters, associated with the slope of the power law decrease of the intensity versus q in the intermediate q range (D_f).

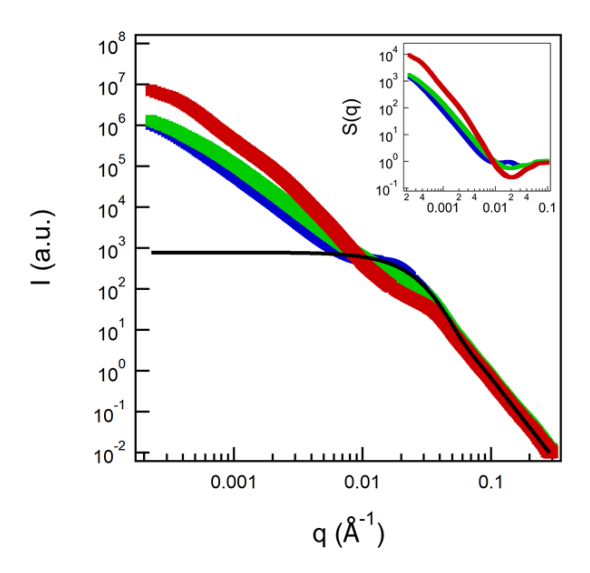


Figure 4: Total scattered intensity for PI-NMP-SiO₂ in PI-Sigma with increasing grafted molecular weights corresponding to Table 1: (red) C1, (green) C2, and (blue) C3. The black line is the calculated form factor for a primary NP of mean radius of 6.5 nm with a log-normal distribution of 0.3. (Inset: Corresponding structure factors calculated by dividing the total intensity by the primary NP form factor.)

We can determine an order of magnitude of the cluster size using the formula $R_{agg}=R_{NP}.N_{agg}^{1/Df}$, corresponding to a lower bound value of cluster size (i.e. the clusters must be at least this size). The apparent aggregation number and the fractal dimension of the clusters are determined graphically from the structure factors in Figure 4 from the extrapolated plateau at low q and from the slope in the intermediate q range and reported in Table 3.

 Table 3: Structure Factor Parameters

Sample	N_{agg}	D_f	R _{agg} (nm)	P/N
C1	8850	2.55	212	1.75
C2	1640	2.35	140	0.92
СЗ	1350	2.26	146	0.78

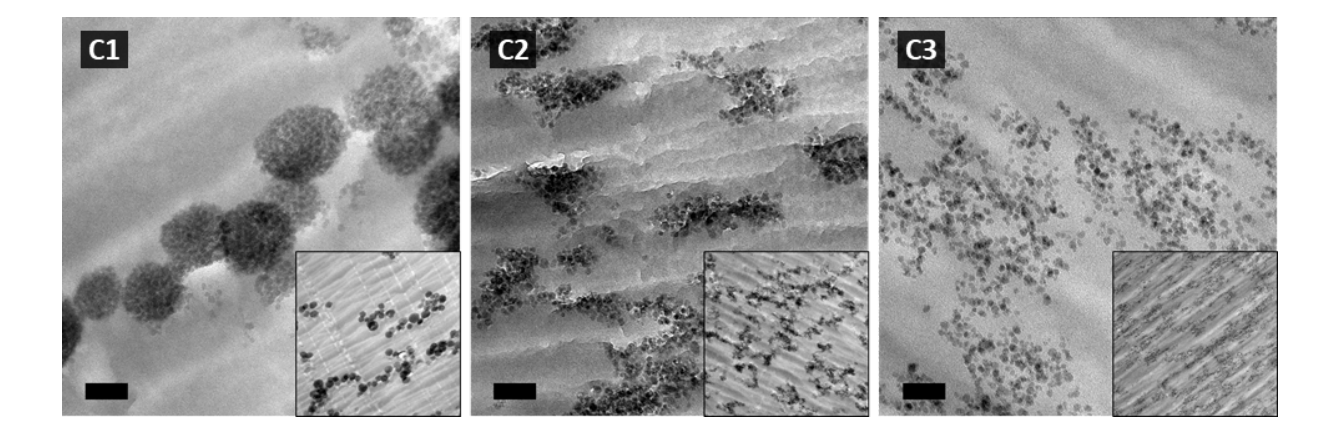


Figure 5: TEM images of PI-NMP-SiO₂ dispersed in the PI-Sigma matrix with P/N values (C1) 1.75, (C2) 0.92, and (C3) 0.78. Scale bar is 100 nm for the large images and 1 μ m for the insets.

Evidently, both the apparent aggregation number and the fractal dimension decrease when P/N decreases, meaning the average size of the clusters is decreasing. The compactness of the clusters is also decreasing, suggesting that they are more ramified. This is further supported with a shift of the particle-particle correlation peak on the structure factor (Figure 4). The peak is initially around 0.04 Å^{-1} , corresponding to two particles in close contact inside the cluster ($d\sim15 \text{ nm}$), and moves to around 0.02 Å^{-1} ($d\sim30 \text{ nm}$) for sample C3, suggesting the particles are moving away from each other with the ramification of the cluster structure. We again supplement this characterization of NP dispersion through the use of TEM images (Figure 5). Images are shown at two different magnifications to representatively portray the structures forming in system at different scales. The images confirm the formation of clusters of average sizes around 200-400 nm – consistent with the average values determined by SAXS. We can clearly see the decreasing of the compactness of the cluster when decreasing the P/N value which is also consistent with the SAXS analysis. It appears that we have an obvious transition of particle dispersion with the increasing grafted polymer length. The first two structures (C1, C2) appear to be fairly compact clusters, while C3

seems to have a more open structure with a fractal dimension close to 2. This system has provided us with detailed analysis of the transition from small clusters to sheets, right near the expected range in the morphology diagram. The moderated mismatch in polymer microstructure appears to have little effect on this expected transition range.

3. Mismatched Chemistry

Taking one last step in understanding the dispersion mechanisms, we now choose to mix the NMP PI grafted NPs into a Styrene-Butadiene-Rubber (SBR) matrix. In order to test the compatibility between the grafted chains and the matrix, relative to that of the PI systems, a DSC analysis was performed on mixtures (50 wt.%) of PI-NMP and PI-sigma as compared with that of mixtures of PI-NMP and SBR (Figure 6). The Tg of PI-sigma was -60 °C, the Tg of PI-NMP was -53 °C, and we observed only one Tg at -58 °C for the mixture. This confirms for us that the two polymers are indeed miscible. We compare this to the same DSC miscibility test of PI-NMP and SBR. In this case the mixture is made with 80 wt.% SBR in order to be representative of the real proportions of the nanocomposites. The results show two separate Tg for the mixture, identical to those of the individual polymers (-53 °C for PI-NMP and -38 °C for SBR), thus indicating the immiscibility between the two systems. This then becomes the first system in this study in which the grafted and free polymer chains are expected to have strong enough interactions to be enthalpically immiscible.

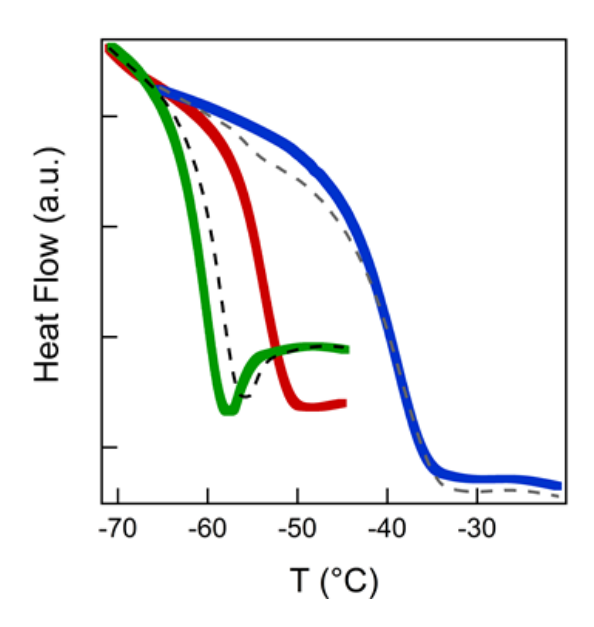


Figure 6: DSC on polymer systems with no NPs showing the glass transitions for (green) PI-Sigma, (red) PI-NMP, (blue) SBR, with the dashed lines corresponding to 50/50 wt.% mixtures of (black) PI-Sigma/PI-NMP and (grey) PI-NMP/SBR.

The resulting structure factors for the NP mixed composites are reported in Figure 7 for the two samples comprised of PI-NMP-SiO₂ in SBR with P/N ratios of 2.88 and 1.49, similar to that of the previous section. We observe that the PI-NMP-NP dispersion is significantly different in the SBR matrix than in the PI-Sigma matrix. The D1 sample presents a lower mean cluster size (100nm) than the corresponding C1 (200 nm) with a larger fractal dimension larger (around 2.7) suggesting that the dispersion corresponds there more closely to the small clusters phase. More surprisingly, we can see that when reducing the P/N value, the SBR system D2 behaves opposite to the PI counterpart (C2) - The scattering intensity goes up, meaning the mean aggregate size increases (150 nm), supplemented by the fractal dimension increase to 3, suggesting more compact aggregates.

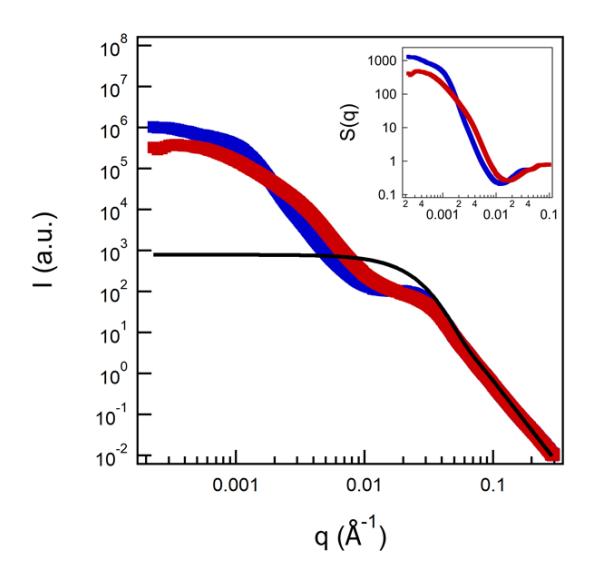


Figure 7: SAXS on PI-NMP-SiO₂ in SBR with P/N values of (red, D1) 2.88 and (blue, D2) 1.49. (Inset: Corresponding structure factors.)

These are notably more compact even than the C1 counterpart which in fact lies closer to the small cluster region on the phase diagram. While the C2 moves as expected to the connected sheet phase, the intensity goes down and the fractal dimension decreases. Such scattering behavior observed for the D2 is characteristic of phase separation which results in large, compact clusters of particles as previously observed for phase separation 13 . This is a clear impact of the enthalpic contribution that seems to dominate the entropic one seen in the microstructure mismatch, even accounting for shifts in the minor shifts in the initial state (i.e. variation over the P/N ratio) compared to the athermal and the moderated mismatched systems. As a result, the dispersion does not follow the predicted structure given by the phase diagram, but rather calls for a shift in the region boundaries to account for the enthalpic contributions.

IV CONCLUDING REMARKS

To summarize, we dispersed the PI grafted particles in a PI matrix of constant molecular weight and showed that the dispersion follows the predicted morphology diagram of Kumar *et al.*¹⁵ only

in athermal conditions (i.e. the matrix and grafted polymer are identical in chemical structure) according to interactions only driven by mixing entropy. We have seen that for the matched microstructure (A), the final dispersion is in close agreement with the one given by the phase diagram. With a small change in the microstructure of the PI matrix (B, C) we observe that the entropic morphology diagram still works, except in regions near boundaries between different morphologies. This is particularly prominent with long grafted chains (B) at moderately high graft densities (the well dispersed region of the phase diagram), which seems to be more sensitive to the change in the matrix. Finally, when dispersing grafted PI particle in a SBR matrix (D), one can see that we lose even qualitative agreement with the expected morphologies presumably due to the dominant contribution of the enthalpic interactions. We believe these results bring new insights in the understanding of the dispersion mechanism in nanocomposites and provides a promising tool when designing controlled grafted elastomers in pursuit of specific desired macroscopic properties. Future work can explore further quantifying the enthalpic effects of the various interactions in the system that could tip the system in favor of dispersion or agglomeration (i.e. NP-NP core attraction, NP-matrix affinity, graft-matrix interaction)^{32,33}.

ASSOCIATED CONTENT

Supporting Information. PI synthesis procedure details, morphology diagram details, SAXS

structure factors.

The following files are available free of charge.

PI_Morphology_SI.pdf

AUTHOR INFORMATION

Corresponding Authors

Jacques Jestin * jacques.jestin@cea.fr

Sanat Kumar * <u>sk2794@columbia.edu</u>

Author Contributions

JJ, DG, NM, TP, SK and MC designed the experiments. MB, AMJ, and DD have prepared all of

the samples. AMJ performed the TEM imaging. All the authors have performed the experiments

and participated in the analysis, interpretation and discussion of the results. The manuscript was

written through the main contribution of AMJ, MB, SK and JJ and has been revised by all the

authors. All authors have given approval to the final version of the manuscript.

ACKNOWLEDGMENTS

We thank NYULMC DART Microscopy Lab for assistance in EM work and ANR Nanointerprop

for funding. SK, DD, and AMJ acknowledge funding from the NSF DMR-1709061.

22

REFERENCES

- ¹ Jayanthi, S.; Arulsankar, A.; Sundaresan, B. NanoSrTiO3-filled PEO–P(VdF-HFP)–LiClO4 electrolytes with improved electrical and thermal properties. *Appl. Phys. A* **2016**, *122* (2).
- ² Althues, H.; Palkovits, R.; Rumplecker, A.; Simon, P.; Sigle, W.; Bredol, M.; Kynast, U.; Kaskel, S. Synthesis and characterization of transparent luminescent ZnS: Mn/PMMA nanocomposites. *Chem. Mater.* **2006**, *18* (4), 1068–1072.
- ³ Jouault, N.; Vallat, P.; Dalmas, F.; Said, S.; Jestin, J.; Boué, F. Well-dispersed fractal aggregates as filler in polymer-silica nanocomposites: long-range effects in rheology. *Macromolecules* **2009**, *42 (6)*, 2031-2040.
- ⁴ Attia, N. F.; Hassan, M. A.; Nour, M. A.; Geckeler, K. E. Flame-retardant materials: synergistic effect of halloysite nanotubes on the flammability properties of acrylonitrile-butadiene-styrene composites. *Polym. Int.* **2014**, *63* (7), 1168–1173.
- ⁵ Liang, Y.; Cao, W.; Li, Z.; Wang, Y.; Wu, Y.; Zhang, L. Effect of octadecylamine modified graphene on thermal stability, mechanical properties and gas barrier properties of brominated butyl rubber. *Polym. Test.* **2008**, *27* (3), 270–276.
- ⁶ Zhao, D.; Gimenez-Pinto, V.; Jimenez, A. M.; Zhao, L.; Jestin, J.; Kumar, S. K.; Kuei, B.; Gomez, E. D.; Shanker Prasad, A.; Schadler, L. S.; Khani, M. M.; Benicewicz, B. C. Tunable Multiscale Nanoparticle Ordering by Polymer Crystallization. *ACS Cent. Sci.* **2017**, 3 (7), 751–758.

- ⁷ Zhao, D.; Ge, S. F.; Senses, E.; Akcora, P.; Jestin, J.; Kumar, S. K. Role of filler shape and connectivity on the viscoelastic behavior in polymer nanocomposites. *Macromolecules* **2015**, 48 (15), 5433-5438.
- ⁸ Jouault, N.; Dalmas, F.; Boué, F.; Jestin, J. Nanoparticles reorganizations in polymer nanocomposites under large deformation. *Polymer* **2014**, 55 (10), 2523-2534.
- ⁹ Robbes, A.-S.; Cousin, F.; Meneau, F.; Dalmas, F.; Boué, F.; Jestin, J. Nanocomposite Materials with Controlled Anisotropic Reinforcement Triggered by Magnetic Self-Assembly. *Macromolecules* **2011**, 44 (22), 8858–8865.
- ¹⁰ Strawhecker, K. E.; Manias, E. Structure and Properties of Poly(vinyl alcohol)/Na+ Montmorillonite Nanocomposites. *Chem. Mater.* **2000**, 12 (10), 2943–2949.
- ¹¹ Schaefer, D. W.; Justice, R. S. How Nano Are Nanocomposites? *Macromolecules* **2007**, *40* (24), 8501–8517.
- ¹² Mishra, S.; Shimpi, N. G. Effect of the variation in the weight percentage of the loading and the reduction in the nanosizes of CaSO4 on the mechanical and thermal properties of styrene–butadiene rubber. *J. Appl. Polym. Sci.* **2007**, *104* (3), 2018–2026.
- ¹³ Chevigny, C.; Dalmas, F.; Di Cola, E.; Gigmes, D.; Bertin, D.; Boué, F.; Jestin, J. Polymer-Grafted-Nanoparticles Nanocomposites: Dispersion, Grafted Chain Conformation, and Rheological Behavior. *Macromolecules* **2011**, 44, 122–133.
- ¹⁴ Robbes, A. S.; Cousin, F.; Meneau, F.; Dalmas, F.; Schweins, R.; Gigmes, D.; Jestin, J. Polymer-Grafted Magnetic Nanoparticles in Nanocomposites: Curvature Effects, Conformation of Grafted

Chain, and Bimodal Nanotriggering of Filler Organization by Combination of Chain Grafting and Magnetic Field. *Macromolecules* **2012**, 45, 9220–9231.

- ¹⁵ Kumar, S. K.; Jouault, N.; Benicewicz, B.; Neely, T. Nanocomposites with Polymer Grafted Nanoparticles. *Macromolecules* **2013**, 46, 3199–3214.
- ¹⁶ Heinrich, G.; Klüppel, M.; Vilgis, T. A. Reinforcement of Elastomers. *Curr. Opin. Solid State Mater. Sci.* **2002**, *6*, 195–203.
- ¹⁷ Utara, S.; Jantachum, P.; Sukkaneewat, B. Effect of surface modification of silicon carbide nanoparticles on the properties of nanocomposites based on epoxidized natural rubber/natural rubber blends. *J. Appl. Polym. Sci.* **2017**, *134*.
- ¹⁸ Nazhat, S. N.; Parker, S.; Riggs, P. D.; Braden, M. Blends of Isoprene-styrene/methacrylate monomer mixtures as potential soft lining material. *Biomaterials* **2001**, *22* (15), 2087–2093.
- ¹⁹ Nazhat, S. N.; Parker, S.; Patel, M. P.; Braden, M. Isoprene-styrene copolymer elastomer and tetrahydrofurfuryl methacrylate mixtures for soft prosthetic applications. *Biomaterials* **2001**, *22* (17), 2411–2416.
- ²⁰ Sandusky, D.; McInnis, E. Alloy blends of polyurethane and rubber. 20040186213, March **2004**.
- ²¹ Almeida, A. P. P.; Oliveira, A. P. L. R. de; Erbetta, C. D. C.; Sousa, R. G. de; Freitas, R. F. de S.; Silva, M. E. S. R. e. Rheological Study of Polymers Used as Viscosity Index Improvers for Automotive Lubricant Oils. *J. Mod. Phys.* **2014**, *05* (12), 1085–1093.

- ²² Dibbanti, M. K.; Mauri, M.; Mauri, L.; Medaglia, G.; Simonutti, R. Probing small network differences in sulfur-cured rubber compounds by combining nuclear magnetic resonance and swelling methods. *J. Appl. Polym. Sci.* **2015**, *132* (43).
- ²³ Mary, C.; Philippon, D.; Lafarge, L.; Laurent, D.; Rondelez, F.; Bair, S.; Vergne, P. New Insight into the Relationship Between Molecular Effects and the Rheological Behavior of Polymer-Thickened Lubricants Under High Pressure. *Tribol. Lett.* **2013**, *52* (3), 357–369.
- ²⁴ Fröhlich, J.; Niedermeier, W.; Luginsland, H.-D. The effect of filler–filler and filler–elastomer interaction on rubber reinforcement. *Compos. Part Appl. Sci. Manuf.* **2005**, *36*, 449–460.
- ²⁵ Bouty, A.; Petitjean, L.; Degrandcourt, C.; Gummel, J.; Kwaśniewski, P.; Meneau, F.; Boué, F.; Couty, M.; Jestin, J. Nanofiller Structure and Reinforcement in Model Silica/Rubber Composites: A Quantitative Correlation Driven by Interfacial Agents. *Macromolecules* **2014**, *47* (15), 5365–5378.
- ²⁶ Bouty, A.; Petitjean, L.; Chatard, J.; Matmour, R.; Degrandcourt, C.; Schweins, R.; Meneau, F.; Couty, M.; Jestin, J. Interplay between polymer chain conformation and nanoparticle assembly in model industrial silica/rubber nanocomposites. *Faraday Discuss.* **2016**, 186, 805 325–343.
- ²⁷ Baeza, G. P.; Genix, A.-C.; Degrandcourt, C.; Petitjean, L.; Gummel, J.; Couty, M.; Oberdisse, J. Multiscale Filler Structure in Simplified Industrial Nanocomposite Silica/SBR Systems Studied by SAXS and TEM. *Macromolecules* **2013**, 46 (1), 317–329.
- ²⁸ Hosseini, S. M.; Torbati-Fard, N.; Kiyani, H.; Razzaghi-Kashani, M. Comparative role of Interface in reinforcing mechanisms of Nano silica modified by Silanes and liquid rubber in SBR composites. *J. Polym. Res.* **2016**, *23* (9).

- ²⁹ Khani, M. M.; Abbas, Z. M.; Benicewicz, B. C. Well-Defined Polyisoprene-Grafted Silica Nanoparticles via the RAFT Process. *J. Polym. Sci. Part A. Polym. Chem.* **2017**, *55* (9), 1493–1501.
- ³⁰ Bonnevide, M.; Phan, T. N. T.; Malicki, N.; Kumar, S. K.; Couty, C.; Gigmes, D.; Jestin, J.; Synthesis of Polyisoprene, Polybutadiene and Styrene Butadiene Rubber grafted silica nanoparticles by Nitroxide-Mediated Polymerization, to be submitted, **2019**.
- 31 Akcora, P.; Liu, H.; Kumar, S. K.; Moll, J.; Li, Y.; Benicewicz, B. C.; Schadler, L. S.; Acehan, D.; Panagiotopoulos, A. Z.; Pryamitsyn, V.; Ganesan, V.; Ilavsky, J.; Thiyagarajan, P.; Colby, R. H.; Douglas, J. F; Anisotropic self-assembly of spherical polymer-grafted nanoparticles, *Nature Materials*, **2009**, 8, 354–359.
- ³² Martin, T. B.; Mongcopa, K. I. S.; Ashkar, R.; Butler, P.; Krishnamoorti, R.; Jayaraman, A. Wetting–Dewetting and Dispersion–Aggregation Transitions Are Distinct for Polymer Grafted Nanoparticles in Chemically Dissimilar Polymer Matrix. J. Am. Chem. Soc., 2015, 137, 10624–10631.
- Zhang, R.; Lee, B.; Bockstaller, M. R.; Kumar, S. K.; Stafford, C. M.; Douglas, J. F.; Raghavan,
 D.; Karim, A. Pattern-Directed Phase Separation of Polymer-Grafted Nanoparticles in a
 Homopolymer Matrix. Macromolecules, 2016, 49, 3965–3974.

Morphologies of Polyisoprene Grafted Silica Nanoparticles in Model Elastomers

Marine Bonnevide, Andrew M. Jimenez, Deboleena Dhara, Trang N.T. Phan, Nicolas Malicki, Zaid Alajeeli, Brian Benicewicz, Sanat K. Kumar, Marc Couty, Didier Gigmes, and Jacques Jestin.

